# Soft Matter

www.softmatter.org

Volume 6 | Number 2 | 21 January 2010 | Pages 197–424

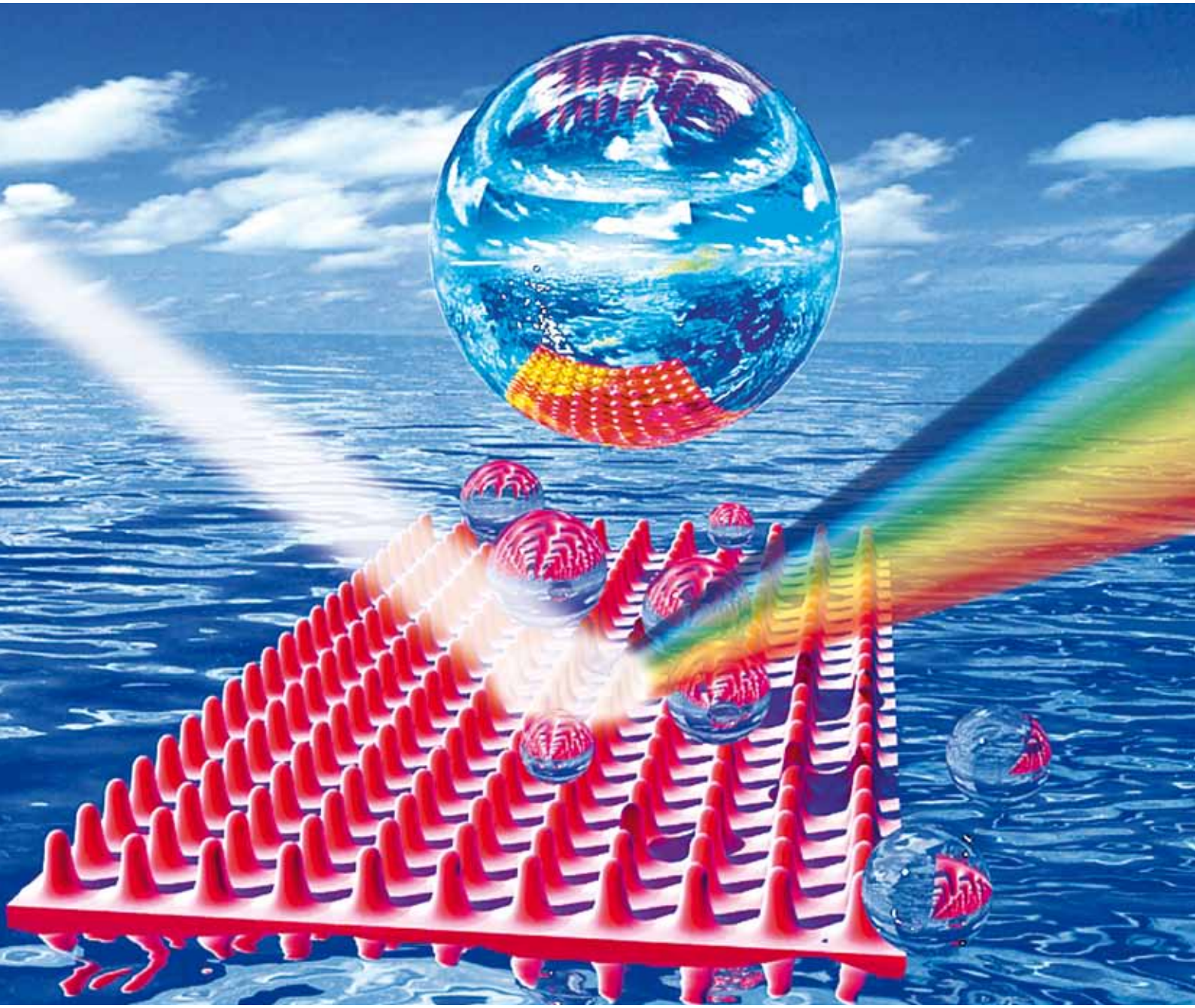

ISSN 1744-683X

RSC Publishing

**PAPER**
Hong-Bo Sun *et al.*
A facile approach for artificial biomimetic surfaces with both superhydrophobicity and iridescence

**REVIEW**
Thomas Fröhlich and Ernst Wagner
Peptide- and polymer-based delivery of therapeutic RNA

1744-683X(2010)6:2;1-Q

# A facile approach for artificial biomimetic surfaces with both superhydrophobicity and iridescence†

Dong Wu,[a] Qi-Dai Chen,[a] Hong Xia,[a] Jian Jiao,[a] Bin-Bin Xu,[a] Xiao-Feng Lin,[a] Ying Xu[a] and Hong-Bo Sun*[b]

*Received 29th May 2009, Accepted 4th November 2009*
*First published as an Advance Article on the web 10th December 2009*
**DOI: 10.1039/b910605g**

Biomimetic surfaces are attracting more and more research attention because of the amazing characteristics of living biological species, such as iridescence in flowers of hibiscus trionum and tulipa, and superhydrophobicity on the lotus leaf. Despite numerous efforts for producing the fascinating micro-nanostructures that present either iridescence or superhydrophobicity, there is almost no reports on artificial surfaces that posses both simultaneously apart from a few examples on self-organized colloidal particles. Here, we report bio-inspired charming photonic surface structures consisting of regular micro-needle arrays covered with nano-metal protrusions, which are prepared by multibeam interference patterning plus electroless plating. The multibeam laser approach features rapidness, simplicity and ease of large-area fabrication, for example fabrication of a uniform area of 600 $mm^2$ took less than 1 min. The attained hierarchical artificial surface layers exhibit not only superhydrophobic ability, but also brilliant iridescence, which may be useful as a novel type of decoration layer for buildings, cars, and even clothes.

## Introduction

Artificial superhydrophobic surfaces have attracted tremendous attention and are used for functional biomimetic applications from water-proof and antifouling clothes,[1,2] friction reduction coatings,[3,4] to microfluidic devices,[5] where the existence of natural forces for surface self-cleaning is vital, as done by a lotus leaf.[6] A variety of materials and techniques have been developed to realize micronanostructured surfaces of high roughness that is crucial for superhydrophobicity (water contact angle, CA > 150°), *e.g.*, porous multilayer films,[7,8] self-assembly,[9,10] carbon nanofibers/tubes,[11–14] ultraviolet curing[15] and electrospinning.[16,17] Although some attained surfaces have reached superhydrophobic ability, they usually don't exhibit structural colors. This may hinder their wide applications because beautiful colors are usually important for decorating clothes, hotels, dancing rooms, art screens and signboards. Iridescence, the change in hue of a surface with different observation angles or the lamp flounce, is one of the main reasons why jewellery, pearls, and diamonds are attractive to people and widely used as ornaments. It widely exists in living things such as the wings of peacocks and butterflies, and the back of the tenebrionidae beetle.[18–21] An ideal decoration layer needs both superhydrophobicity and brilliant iridescence to prevent the colorful surface from being polluted. Although realization of such highly functional surfaces is technically challenging, some research groups have begun to create superhydrophobic materials with various colors by self-orgnization of colloidal spheres, for which the key is long-range order of spheres. Gu *et al.* fabricated inverse opal films with both structural color and superhydrophobic ability (CA = 155°) in 2003.[22] However, the opal structure is fragile, and the fabrication process is time-consuming and needs rigorous conditions (450 °C). Jiang and coworkers[23] reported high reflection polystyrene colloidal crystal films, but with a relatively low hydrophobicity (CA ~ 125°). Furthermore, both of the surfaces reported above only show a single color. Apparently, a convenient technology that is able to rapidly produce large-area micronanostructured biomimetic surfaces with both superhydrophobicity and iridescence is desired.

Multibeam interference lithography provides a promising approach for the fabrication of large-area periodic two-dimensional (2D) and three-dimensional (3D) micronanostructures rapidly and cheaply. It has been used for producing 2D gratings, 3D photonic crystals,[24] and flower-like arrays.[25] These structures have demonstrated good optical properties as expected, but they are not appropriate for superhydrophobic applications because of their low roughness surface morphology. So far, it has been unclear whether interference lithography can be used for preparing biomimetic micronanostructures that incorporates both iridescence and superhydrophobicity. Here our study give a positive answer. Periodic nanoneedle arrays were realized by interference lithography and show both iridescence and superhydrophobicity. Furthermore, hierarchical structures were obtained by an additional electroless plating of silver nanoparticles on the needle surfaces to further improve the superhydrophobic ability.

## Experimental

### Laser exposure for patterns formation

A glass slide was cleaned with acetone and absolute ethanol and the photoresist (Norland: NOA 61) diluted with acetone (1 : 1 by volume) was spin-coated at different rotation speeds: 500 rpm for 3 μm, 1000 rpm for 1.5 μm, 3000 rpm for 0.8 μm, and 6000 rpm for

[a]*State Key Laboratory on Integrated Optoelectronics, College of Electronic Science and Engineering, Jilin University, 2699 Qianjin Street, Changchun 130012, China. E-mail: hbsun@jlu.edu.cn; hbsun@ieee.org*
[b]*College of Physics, Jilin University, 119 Jiefang Road, Changchun 130023, China*

† Electronic supplementary information (ESI) available: Supplementary movies 1–3. See DOI: 10.1039/b910605g

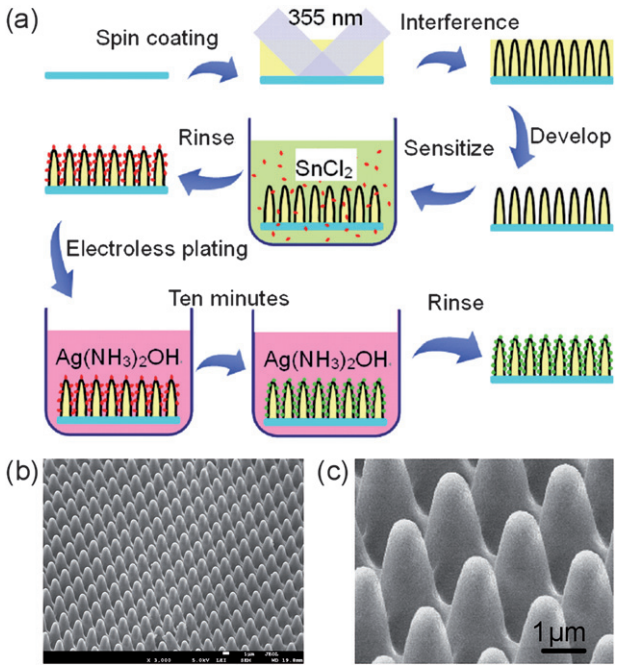


**Fig. 1** Scheme of fabrication of the biomimetic photonic material. (a) The main fabrication process: laser interference, sensitization and electroless plating. (b) SEM image of the nanoneedle arrays fabricated by multibeam laser interference. (c) Magnified SEM image of the nanoneedle arrays. The tip of the needle is about 300 nm radius.

300 nm thicknesses. A frequency-tripled, Q-switched, single-mode Nd:YAG laser (Spectra-physics) with about 10 ns pulse width was split into four beams (wavelength $\lambda = 355$ nm; beam size ~9 mm, and laser power ~100 mW). The beamlets were overlapped on the sample both temporally and spatially to produce designed interference patterns by adjusting the optical path length rigorously (Fig. 1a). The light patterns were converted to matter structures by photopolymerization of the resist at sites of light intensity maximum. After exposure, the samples were developed in acetone for 1 min to remove the unpolymerized resin and the resulting micronanostructures were left. It is worth to mention that the laser exposure of a sample of area of 600 $mm^2$ took less than 1 min. Such a rapid fabrication is not possible by any current available technology. The surface of the sample was further modified with a fluoroalkylsilane ($CF_3(CF_2)_5CH_2CH_2SiCl_3$) by means of thermal chemical vapor deposition for 2 h at 60 °C, to render the surface hydrophobic. CAs were measured using an OCA20 system (Dataphysics GmbH, Germany). First, the water droplet was pulled out from the syringe, then the sample was hoisted until it contacted with the water droplet. At last, a photo was taken and the CA was deduced. Every sample was measured three times to ensure the measurement precision and the average CA was considered as the final static CA. A digital camera was used for imaging and recording the iridescence. The morphologies of the nanoneedle arrays were investigated by field emission scanning electron microscopy (SEM).

### Electroless plating

First, the laser-patterned polymer nanoneedle arrays were sensitized with 10 g $l^{-1}$ $SnCl_2$ solution for 6 min, and then $SnCl_2$ particles were grown and absorbed onto needle surface. Second, the samples were put into the mixed solution of 0.05 mol $l^{-1}$ $Ag(NH_3)_2OH$ and 0.18 mol $l^{-1}$ $NaOOC(CHOH)_2COOK \cdot 4H_2O$ that is used as reducer. Ag particles were replaced with $Sn^{2+}$ and such Ag particles functioned as seeds for nanocrystal growth. A layer of 20 nm Ag was formed on the surface of the needles in 10 min. The sample was rinsed by de-ionized water and dried. Finally, it was modified with fluoroalkylsilane to lower its surface energy.

## Results and discussion

### Regular nanoneedle arrays

According to the Cassie–Baxter model,[26] the smaller the contact area between the surface and the water droplet is, the larger the CA is. In our previous study, we fabricated photonic crystals,[27] pillars and nanonetworks[28] by laser interference. The vision of the current research is to further study the performance of surfaces according to the requirement of superhydrophobicity. Shown in Fig. 1b is the nanoneedles' structure obtained by controlling the exposure time and the thickness of the resin. The morphology of the needles with nanotips significantly reduces the contact area between the surface and the water droplet, and has better hydrophobicity than the common cylindrical pillars. The periodicity $d$ of the pillar in an array is determined by the interference angle $\theta_{air}$ (the angle between the main optical axis and the beamlets) and the wavelength $\lambda$. Given $\theta_{air} = 5.8°$, we have $d = \lambda/(\sqrt{2}\sin\theta_{air}) = 2.5$ μm. The height of the needle is about 3 μm, determined by the thickness of the resin. The tip radius of the needle is only $R = 250$ nm. As predicted by the Cassie–Baxter model,[26] the relation between the apparent contact angle[29] $\theta_r$ and the ideal angle $\theta$ of a flat surface is:

$$\cos\theta_r = r_f f\cos\theta + f - 1 \quad (1)$$

where $f$ is the area fraction of the projected wet area. The product $r_f f$ is often called the solid fraction, $\Phi_s$. Assuming that the water does not invade the roughness, then $r_f f = 1$ and $\Phi_s = f$. In the current research, the solid fraction $\Phi_s = \pi R^2/d^2$, where $d$ is center-to-center pitch. The smaller the solid fraction is, the better the hydrophobic ability is. Given $R = 250$ nm, $d = 2.5$ μm, and $\theta = 110°$, we have $\Phi_s = 0.03$ for the needle while the solid fraction is about 0.16 for the previous reported pillars. The theoretical CA is 168°.

### Superhydrophobicity of the nanoneedle arrays

After the sample was modified with a fluoroalkylsilane ($CF_3(CF_2)_5CH_2CH_2SiCl_3$) by thermal chemical vapor deposition, we investigated the water droplet behavior on the surface (Fig. 2a). First, a 4 μl water droplet (image 1) was approaching the nanoneedle array as the base was gradually hoisted. In image 2, the droplet began to touch with the surface. Due to the needle morphology, the water did not spread out. When the base continued to rise, the tubule exerted force on the water by its surface tension. As shown in image 3, the shape of the water droplet turned into an ellipse while the natural one without external force on superhydrophobic surface was spherical. The water did not spread out even when it was pressed. It is

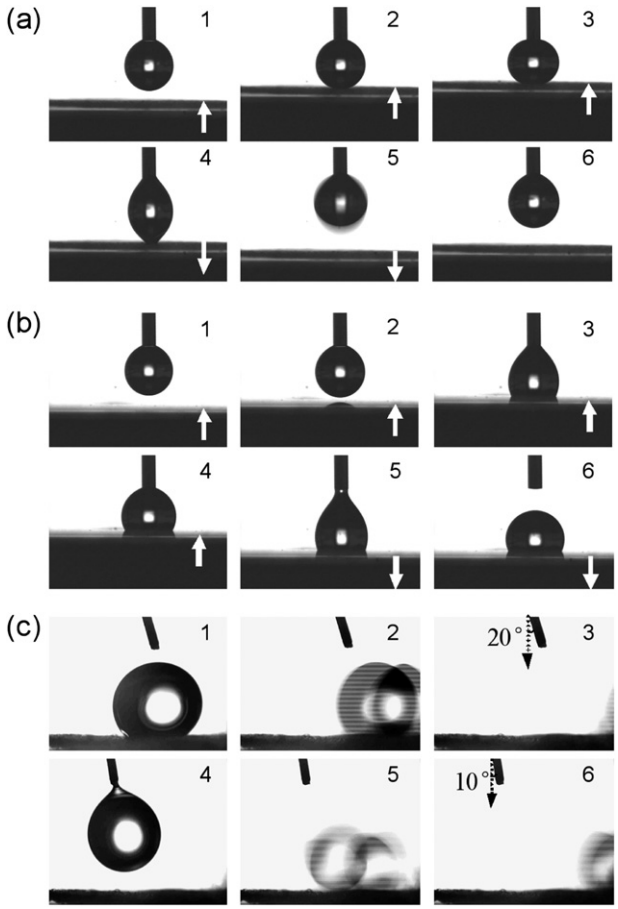


**Fig. 2** Water droplet motion behaviors on modified nanoneedle arrays and flat surfaces. (a) A series of images about a 4 μl water droplet on needle arrays modified by a fluoroalkylsilane to render hydrophobic surface. At first, the water droplet is approaching the surface, and then begins to touch. In image 3, the tubule exerted force on the water by its surface tension and the shape of the water turned into an ellipse. At last, the water was pulled back without any loss. (b) A series of images of water droplet motion behaviors on a flat surface without microstructures. The water sticks to the surface. The white arrow represents the motion direction of the sample. (c) The measurement of advancing, receding angles and roll-off angle.

interesting to note that the water was dragged back without any remnant when the base declined (images 4–6). This is of great importance for applications in the transport of microdroplets.[30] In contrast, on a flat modified surface, once the water droplet touched the surface, it spread out rapidly (image 3, Fig. 2b). The water sticks to the flat surface tightly and can not be pulled back (images 5, 6). The measured CA was 110° ± 2° (image 6, Fig. 2b) while the one for the nanoneedle arrays reached as much as 158° ± 2° (image 3, Fig. 2a). The measured value was a little lower than the theoretical one, which may be caused by the solid fraction. In fact, the water droplet invaded the surface roughness slightly due to its weight[31] and this leads to the increase of the contact area and the coefficient $r_f$. To further investigate its superhydrophobic properties, we tilted the surface (image 1, Fig. 2c) for water droplet rolling down. When the tilted angle was 20°, the water droplet began to roll (image 2 and 3, Fig. 2c). For our measurement system, the CCD and sample were rotated simultaneously, so the image that we took always looked like it was horizontal. But, the syringe didn't move, and it became tilted (image 3) when the sample was rolled. The advancing and receding angles was measured at about 165° ± 3° and 146° ± 2°. The apparent CA was calculated as 154° according to the formula,[29] which agreed well with the measured static contact angle. The roll-off angle was a little large because the tip of the needle was thick. As we know, nanostructures[32] or nanotips[33] of several nanometres were crucial for low roll-off angles and low water adhesion. Moreover, the water could roll down when it was dropped onto the superhydrophobic surface which had been only tilted for 10° (images 1–3, Fig. 2c). This demonstrates that the superhydrophobic surface which may be in a transitional state[34] could be used for *anti*-wetting applications.

### Iridescence of the nanoneedle arrays

Due to the scattering and diffraction of the ordered nanoneedle arrays, the structured surface shows multicolors that are clearly observed by the naked human eye (the inset of Fig. 3a)

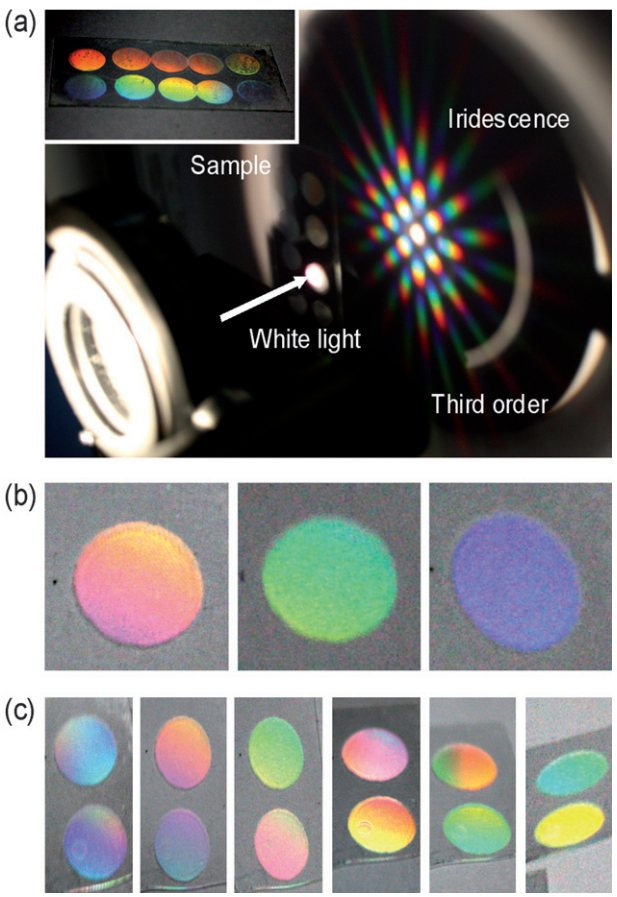


**Fig. 3** Diffraction patterns and iridescence images of the nanoneedle arrays. (a) A photo of the measured experiment. The two-dimensional iridescence is caused by the diffraction of the needle arrays. Every spot is composed of seven colors from red to purple. The inset is a glass substrate with ten samples which are rapidly fabricated within 1 min. (b) The iridescence: red, green and purple which was clearly observed by naked eyes from the same sample under different viewed angles. (c) Brilliant iridescences from two samples with the angles decreasing gradually.

Particularly, the striking surface is iridescent and the color changes from long wavelength red to green, to the short wavelength purple (Fig. 3b) under different viewed angles. For natural species, the brilliant iridescence is known to be important in pollinator attraction, species recognition, mate selection and protection.[35] According to diffraction theory, the interference field is quantitatively described by the grating equation $m\lambda = \delta(\sin\theta_d - \sin\theta_I)$, where $\delta$ is the periodicity of the needle array, $\theta_I$ is the incidence angle, $\theta_D$ is the specular signal and $m$ is the diffraction order. It is surface striations of particular amplitude and frequency that cause interference and give rise to an angular color variation. Yet, the single structural color reported by Sato and coworkers[22] was determined by the optical stop band. Over a range of smaller incident angles, the complete visible spectrum was reflected to the human eye, just like those natural iridescences.[18–21] Shown in Fig. 3c is a series of photos on brilliant iridescence when the viewed angle decreases. When the needle arrays were illuminated with white light from a halogen lamp, a 2D iridescence was observed clearly (Fig. 3a), while the one-dimensional iridescence reported by Steiner and coworkers[35] resulted from grating on the flowers of Hibiscus trionum. Both strong first-order ($m = 1$) and second-order ($m = 1$) interferences are clearly shown, and even the weak third-order ($m = 3$) signal is visible.

### Needle arrays with different heights and widths

The nature of interference lithography offers the unique merit of systemically investigating the effect of structural parameters. Shown in Fig. 4a–c are the needle arrays with different heights 300 nm, 1 μm, and 1.5 μm, respectively. The measured CAs are about 132° ± 3°, 151° ± 1°, and 156° ± 2°. We find that when the height is larger than 1 μm, it has little effect on the hydrophobic ability. However, when the height is below 1 μm, the CA dramatically decreases to 144° ± 2° for 800 nm, 136° ± 1° for 300 nm, and 125° ± 2° for 100 nm heights, respectively. This is because the decrease of the height leads to the reduction of the roughness factor. Besides the needle's height, the effect of needle diameter was also studied. The laser exposure dosage has a dramatic effect on the structure shape. For low exposure dosage, most of the photoresist was washed out or the needle was so thin that it collapses during the developing process. For high exposure dosage, the needles became the rods (Fig. 4d) and even connected with each other (Fig. 4e and f). This resulted in the decrease of the solid fraction. The CAs for three kinds of rods were 148° ± 3°, 136° ± 2°, and 125° ± 1° (the lower insets in Fig. 4d–f), which agreed with the theoretical value of 151° ± 1°, 142° ± 2°, and 132° ± 3° for the tip radius of the rod 600 nm, 800 nm, and 1000 nm, respectively. We find that only needle structures exhibit CAs > 150°, showing that the needle morphology with high surface roughness was crucial for obtaining superhydrophobicity.

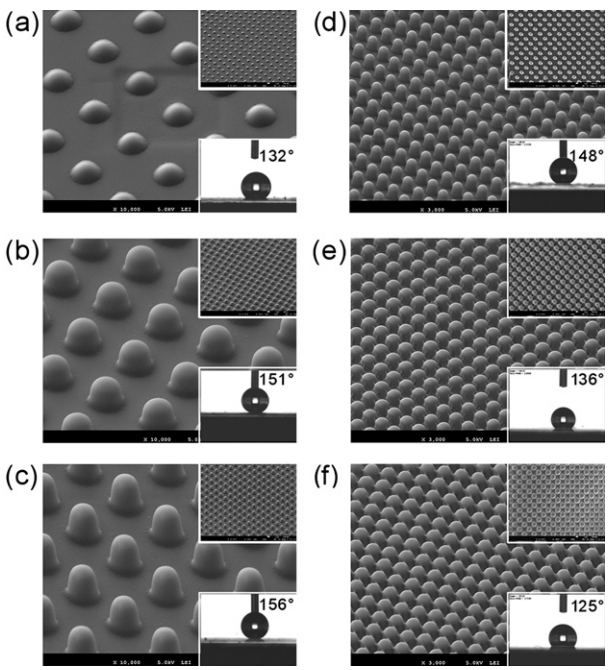


**Fig. 4** The relationship between the height and diameter of the needle arrays and the contact angles. (a)–(c) Titled SEM images of the needle arrays with different heights 300 nm, 1 μm, and 1.5 μm, respectively. The lower insets are the water CA with about 132°, 151° and 156°. (d)–(f) Titled SEM images of the needle arrays with different tip radius 600 nm, 800 nm, and 1000 nm, respectively. The upper inset is the birds-eye SEM views of the needle arrays and the lower insets are the measured CAs with about 148°, 136°, and 125°, respectively.

### Hierarchical structures

To further enhance the superhydrophobicity, we added nano-scaled features on the patterned surfaces to form hierarchical structures, which have been observed in nature and so far widely studied.[36–38] However, most methods for constructing biomimetic hierarchical structures usually require specialized equipment or complicated processing. Electroless plating is a simple, cost-effective, large-area and rapid technique, whereby metal nanoparticles are achieved in ambient conditions. From the magnified image (Fig. 5b and c), we can see that Ag particles with diameters of about 20–50 nm were deposited on the nanoneedle. By this means the surface roughness were further enhanced and the measured CA reached as high as 163° ± 2° (Fig. 5d).

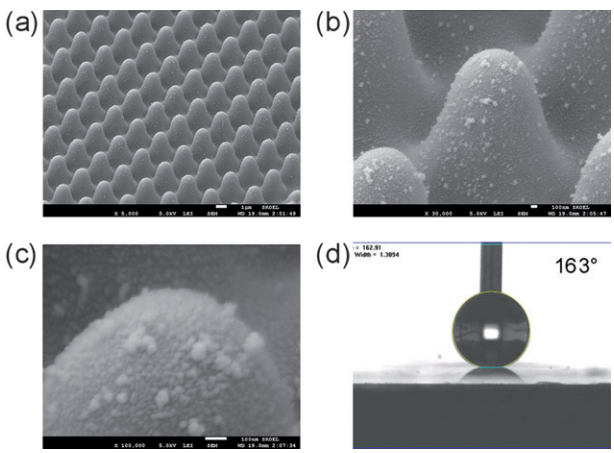


**Fig. 5** The multiscale hierarchical structures obtained by combining interference lithography with electroless plating. (a) Large-area SEM image of the needle arrays with Ag nanoparticles. (b) Enlarged SEM view of a single needle. (c) SEM image of Ag nanoparticles diameter with about 20–50 nm. (d) The water CA measurement.

## Conclusion

We fabricated large-area biomimetic hierarchical structures with both superhydrophobicity and iridescence by using a multibeam interference lithography technology, which features rapid fabrication, and a simple setup, and convenience in operation. Our results show that both the superhydrophobic ability and iridescence of the patterned surfaces are comparable to those found in nature. In addition, the iridescent superhydrophobic surface could be either directly used as a template for PDMS mass production, for example, by soft imprint lithography,[39] or implemented after pattern transfer to hard materials by plasma etching.[40]


## Acknowledgements

The technical help for measurement of CAs and discussion on surface hydrobility from Prof. Wen-Sheng Yang's group, College of Chemistry, Jilin University, is important for the current research. The authors gratefully acknowledge support from the NSFC under grant No. 60525412 and 60677016.


## References


1 P. Gould, *Mater. Today*, 2003, **6**, 44.
2 A. Nakajima, K. Hashimoto and T. Watanabe, *Monatsh. Chem.*, 2001, **132**, 31.
3 P. Ball, *Nature*, 1999, **400**, 507.
4 R. Truesdell, A. Mammoli, P. Vorobieff, F. V. Swol and C. J. Brinker, *Phys. Rev. Lett.*, 2006, **97**, 044504.
5 B. Zhao, J. S. Moore and D. J. Beebe, *Science*, 2001, **291**, 1023.
6 W. Barthlott and C. Neinhuis, *Planta*, 1997, **202**, 1.
7 L. Zhai, F. C. Cebeci, R. E. Cohen and M. F. Rubner, *Nano Lett.*, 2004, **4**, 1349.
8 L. Zhai, M. C. Berg, F. C. Cebeci, Y. Kim, J. M. Milwid, M. F. Rubner and R. E. Cohen, *Nano Lett.*, 2006, **6**, 1213.
9 J. T. Han, Y. Zheng, J. H. Cho, X. Xu and K. Cho, *J. Phys. Chem. B*, 2005, **109**, 20773.
10 I. A. Larmour, G. C. Saunders and S. E. J. Bell, *Angew. Chem., Int. Ed.*, 2008, **47**, 5043.
11 J. Li, S. Sambandam, W. Lu and C. M. Lukehart, *Adv. Mater.*, 2008, **20**, 420.
12 L. Ci, S. M. Manikoth, X. Li, R. Vajtai and P. M. Ajayan, *Adv. Mater.*, 2007, **19**, 3300.
13 Z. Wang, L. Ci, L. Chen, S. Nayak, P. M. Ajayan and N. Koratkar, *Nano Lett.*, 2007, **7**, 697.
14 S. Strinivasan, V. K. Praveen, R. Philip and A. Ajayaghosh, *Angew. Chem., Int. Ed.*, 2008, **47**, 5750.
15 Z. Luo, Z. Zhang, L. Hu, W. Liu, Z. Guo, H. Zhang and W. Wang, *Adv. Mater.*, 2008, **20**, 970.
16 M. Ma, M. Gupta, Z. Li, L. Zhai, K. K. Gleason, R. E. Cohen, M. F. Rubner and G. C. Rutledge, *Adv. Mater.*, 2007, **19**, 255.
17 L. Jiang, Y. Zhao and J. Zhai, *Angew. Chem., Int. Ed.*, 2004, **43**, 4338.
18 P. Vukusic, J. R. Sambles and C. R. Lawrence, *Nature*, 2000, **404**, 457.
19 P. Vukusic, J. R. Sambles, C. R. Lawrence and R. J. Wootton, *Nature*, 2001, **410**, 36.
20 A. R. Parker, V. L. Welch, D. Driver and N. Martini, *Nature*, 2003, **426**, 786–787.
21 A. E. Seago, P. Brady, J. P. Vigneron and T. D. Schultz, *J. R. Soc. Interface*, 2009, **6**, S165, DOI: 10.1098/rsif.2008.0354.focus.
22 Z. Z. Gu, H. Uetsuka, K. Takahashi, R. Nakajima, H. Onishi, A. Fujishima and O. Sato, *Angew. Chem., Int. Ed.*, 2003, **42**, 894.
23 H. Ge, Y. Song, L. Jiang and D. Zhu, *Thin Solid Films*, 2006, **515**, 1539.
24 M. Campbell, D. N. Sharp, M. T. Harrison, R. G. Denning and A. J. Turberfield, *Nature*, 2000, **404**, 53.
25 D. Wu, Q. D. Chen, B. B. Xu, J. Jiao, Y. Xu, H. Xia and H. B. Sun, *Appl. Phys. Lett.*, 2009, **95**, 091902.
26 A. B. D. Cassie and S. Baxter, *Trans. Faraday Soc.*, 1944, **40**, 546.
27 S. Shoji, H. B. Sun and S. Kawata, *Appl. Phys. Lett.*, 2003, **83**, 608.
28 H. B. Sun, A. Nakamura, S. Shoji, X. M. Duan and S. Kawata, *Adv. Mater.*, 2003, **15**, 2011.
29 A. Marmur, *Soft Matter*, 2006, **2**, 12.
30 X. Hong, X. F. Gao and L. Jiang, *J. Am. Chem. Soc.*, 2007, **129**, 1478.
31 Z. Yoshimitsu, A. Nakajima, T. Watanabe and K. Hashimot, *Langmuir*, 2002, **18**, 5818.
32 Y. Lai, X. Gao, H. Zhuang, J. Huang, C. Lin and L. Jiang, *Adv. Mater.*, 2009, **21**, 3799.
33 E. Hosono, S. Fujihara, I. Honma and H. Zhou, *J. Am. Chem. Soc.*, 2005, **127**, 13458.
34 S. Wang and L. Jiang, *Adv. Mater.*, 2007, **19**, 3423.
35 H. M. Whitney, M. Kolle, P. Andrew, L. Chittka, U. Steiner and B. J. Glover, *Science*, 2009, **323**, 130.
36 Y. Lee, S. H. Park, K. B. Kim and J. K. Lee, *Adv. Mater.*, 2007, **19**, 2330.
37 S. J. Choi, K. Y. Suh and H. H. Lee, *J. Am. Chem. Soc.*, 2008, **130**, 6312.
38 J. Hong, W. K. Bae, H. Lee, S. Oh, K. Char, F. Caruso and J. Cho, *Adv. Mater.*, 2007, **19**, 4364.
39 F. Hua, Y. Sun, A. Gaur, M. A. Meitl, L. Bihaut, L. Rotkina, J. Wang, P. Geil, M. Shim and J. A. Rogers, *Nano Lett.*, 2004, **4**, 2467.
40 W. L. Min, B. Jiang and P. Jiang, *Adv. Mater.*, 2008, **20**, 3914.